

Simulating Raman Spectra using molecular dynamics, and identification of high-pressure phases III and IV in hydrogen

Ioan B. Magdău and Graeme J. Ackland
 CSEC, SUPA, School of Physics and Astronomy,
 The University of Edinburgh, Edinburgh EH9 3JZ, UK
 (Dated: November 25, 2021)

We present a technique for extracting Raman intensities from *ab initio* molecular dynamics (MD) simulations at high temperature. The method is applied to the highly anharmonic case of dense hydrogen up to 500 K for pressures ranging from 180 GPa to 300 GPa. On heating or pressurizing we find first-order phase transitions at the experimental conditions of the phase III - IV boundary. Direct comparison of Raman vibrons with experiment provides excellent discrimination between subtly different structures, found in MD. We find candidate structures whose Raman spectra are in good agreement with experiment. The new phase obtained in high temperature simulations adopts a dynamic, simple hexagonal structure with three layer types: freely rotating hydrogen molecules, static hexagonal trimers and rotating hexagonal trimers. We show that previously calculated structures for phase IV are inconsistent with experiment, and their appearance in simulation is due to finite size effects.

There have been some notable recent successes of using total energy calculations based on density functional (DFT) to calculate expected signals from candidate structures, for comparison with inconclusive experimental data. Agreement provides validation of the DFT structure, and this combined approach can yield more information, with higher reliability, than either technique alone.

Raman spectroscopy provides one such experimental probe, applicable in extreme conditions but providing insufficient data to determine crystal structure or identification of the vibrational mode [1, 2]. Reliable calculation of Raman frequencies and intensities of mechanically stable structures can be obtained using density functional perturbation theory (DFPT) [3, 4] based on *ab initio* lattice dynamics (LD) [5, 6]. However these methods do not include high temperature effects, and fail for dynamically-stabilized structures with imaginary phonon frequencies. One solution to this is to extract vibrational frequencies from molecular dynamics (MD) data [7–10].

For simple structures this is relatively straightforward; *bcc* titanium and zirconium being nice examples. In these materials the soft T_{1N} phonon eigenvector is well defined, and its frequency and width can be calculated from projection of the MD (or Monte Carlo) trajectories onto the relevant mode eigenvector, followed by Fourier Transform (FT) [8, 11].

In lower-symmetry molecular systems there may be many modes which are formally Raman active, and the coupling between lattice and molecular modes is typically highly temperature-dependent. Worst of all are plastic crystal phases where the molecules can reorient in MD and the eigenvectors calculated from perturbation theory become totally irrelevant.

In this Letter we present a method for calculating Raman frequencies from molecular dynamics, and apply it

to the particularly awkward and topical case of the high-frequency vibron modes in high pressure hydrogen.

Although liquid and solid phases I, II of hydrogen have been well studied using MD [12–14], much interest recently has focussed on pressures around 200-300 GPa where several phases are reported. Generally accepted are a low temperature phase III [15] and a high temperature phase IV [16, 17]. Theoretical predictions of many other phases [18, 19] have been made, and Raman data suggests phase IV may itself have a subtle structural change at 270 GPa [20].

At these pressures x-ray experiments are exceedingly difficult, while neutron diffraction is simply impossible; therefore most experimental data are extracted from Raman and infrared spectroscopy, alongside conductivity measurements. None of these techniques produce enough data to resolve crystal structures, so DFT studies have also been attempted [17–19]. Although these calculations typically ignore quantum effects on the protons, they still provide a useful indication of the likely structures. Very recent papers [21, 22] applying path integral MD to high pressure hydrogen show no qualitative behavioural change to the phase diagram: the main effect is that tunnelling allows molecular rotations to occur at slightly lower temperatures than in classical MD, lowering the phase lines. Most importantly for the present work, the vibrational frequencies of the molecules are largely unchanged by the path integral dynamics.

Enthalpy is easily calculated in DFT, being the combination of total energy of binding of electrons to atoms, plus the zero point energy. Phase III should be the lowest enthalpy phase over a wide range of pressures. *Ab initio* structure search [19] unveiled a number of candidate phases with low total energy, and evaluation of normal modes, phonon frequencies and zero point energy gave rise to prediction of a $C2/c$ symmetry phase. From the phonon calculation it is further possible to calculate

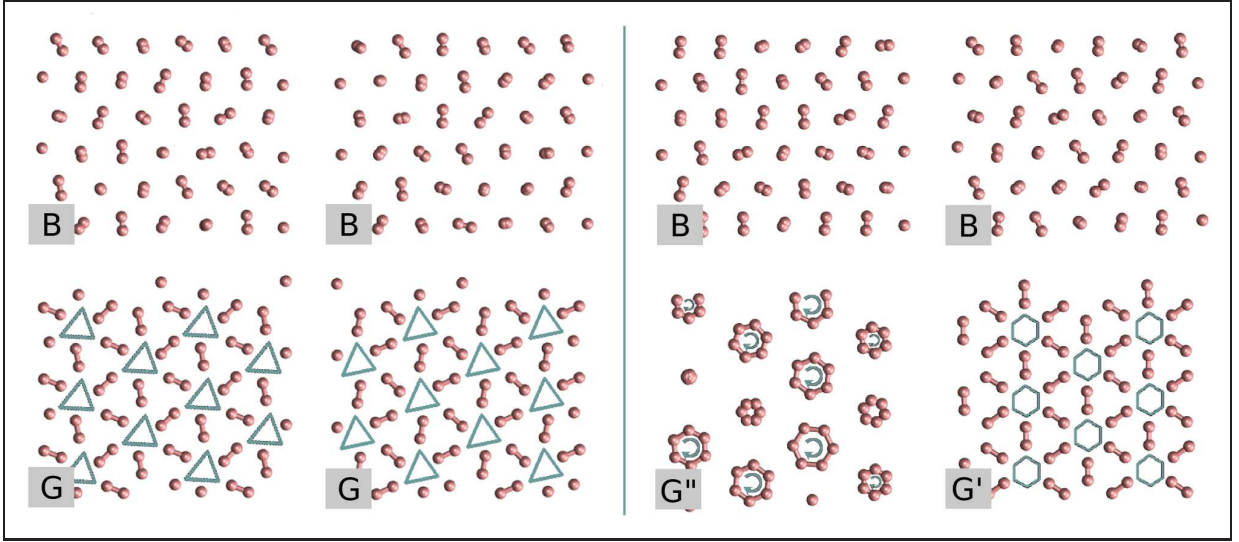


FIG. 1. Time-averaged (1ps) atomic positions from simulations at pressure/temperature/initial configuration. Left column: phase IVa, stacked $BGBG$, 220 GPa / 220 K / Pc ; right column: phase IVb, stacked $BG''BG'$, 270 GPa / 220 K / Pc . The time averaging is chosen large enough to capture the rotation of the B -layer molecules and G'' -layer motifs making these smaller, but not so large that the motifs become points at the central position (representing 2 (B) and 6 (G'') atoms respectively). Note the strong 6-fold symmetry in phase IVb compared with IVa. Many other similar figures are given in [27], showing the trends with P and T .

polarization and polarizability, from which Raman and infrared intensities may be deduced. These show reasonable agreement between $C2/c$ and experiment for phase III [19, 23–26].

Phase IV exists at higher temperatures and is therefore stabilized by entropy. High temperature calculations are more challenging for DFT. Using the quasiharmonic approach based on zero-temperature calculations, Pickard et al [17] evaluated free energies at finite temperature to claim that phase IV should be a layered structure with alternating graphene-like hexagonal layers interspersed with ordered molecular layers and Pc symmetry. We refer to these layers as G and B -type respectively. The critical result here is that the two different layers give strongly Raman active vibron modes at two very different frequencies. Experimental work also finds two vibron modes, lending support to a two-layer model [16].

We have extended these calculations of enthalpies and phonons using the CASTEP code [28] across a wider range of frequencies and with a variety of pseudopotentials (both ultrasoft and norm-conserving with various tunings) and exchange-correlation functionals. We find that these previous results are robust [29]. Despite qualitative agreement, the lower-frequency vibron is observed at much higher frequency than calculated, and with very large width (Fig.2 and [27]). We also used static calculations to investigate whether the G layers have atomic or molecular character. Mulliken bond analysis shows very clearly that the G -layer hexagonal are rings of three H_2 molecules: the Mulliken charge in the molecular bond is at least double that between molecules (1.5e vs 0.3e at

180 GPa, closing to 1.3e to 0.65e at 350 GPa). This result is consistent with snapshots from MD. The reduction in molecular fidelity with pressure is accompanied by a steady reduction in the band gap.

We have conducted a range of MD simulations at various conditions of temperature and pressure, starting in either the Pc or the $C2/c$ phase. We find that simulations with 48 atoms are plagued with finite size effects for reasons explained in [27], so all data here come from 288-atom calculations. The unit cells of Pc and $C2/c$ are sufficiently dissimilar that transformation between the two does not occur. This makes it clear that MD alone cannot be relied upon to find the experimental structure: comparison with data is essential for validation. However, we do observe direct phase transformation in the MD between layered structures with and without the B -type free rotating molecular layer.

In simulations starting in $C2/c$ we find a stable G -layered structure at temperatures up to around 300 K, above which a transformation occurs to a structure with alternating B and G layers similar to the monoclinic $C2$ [19]. The transformation mechanism is such that the $GBGB$ -structure layers become almost orthogonal to the original $C2/c$ [27].

For simulations starting in Pc , we find reversible transitions between two phases: a structure with $BGBG$ stacking similar to Pc , with threefold layer-symmetry but with the B -layer molecules rotating about their centres, and a high-temperature structure with hexagonal symmetry, stacked $BG'BG''$ with sixfold layer-symmetry where the G' layer has hexagonal symmetry and the G''

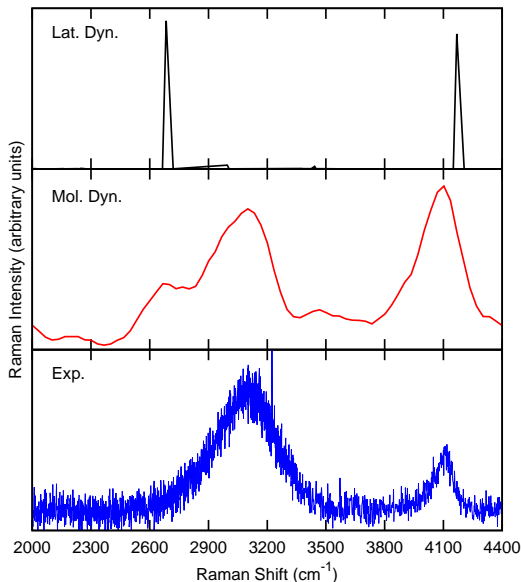


FIG. 2. Comparison of Raman spectra at 270 GPa: Top DFPT lattice dynamics calculation (0 K); Middle MD calculation of Raman signal from IVb at 220 K; Bottom, experimental data at room temperature from Howie et al [16]. Note that the sensitivity of the detector is reduced at high frequency [20], so the peak amplitudes are not directly comparable.

layer exhibits fast rebonding which enables rotation of the hexagonal motifs of three hydrogen molecules. We refer to these phases as IVa and IVb (Fig.1). This transition is observed in two ways [27]: a single MD run with a ramped temperature rise and subsequent decrease traverses a path IVa - IVb - IVa with little hysteresis; alternately, calculations at fixed T and P show the two phases. We use these latter calculations as the basis for our Raman calculations, to test the simulated structures against experiment. It should be noted that our simulations have only four layers, so more complex stackings may exist.

Our DFPT-LD calculations show that all modes in the *Pc* phase are Raman active. To compare with experiment we initially tried projecting the MD trajectories onto LD eigenmodes, multiplying by the calculated Raman intensity and taking the Fourier Transform [27]. This method relies on the normal mode vectors being invariant over time and with temperature. At the lowest temperature, 60 K, the structure remains in the initial configuration (metastable *Pc*) and the projection method gives a Raman signal in precise agreement with LD, as it should for harmonic vibrations [27]. At higher temperatures molecular rotations exchange atom positions, and this method fails.

Closer inspection shows that the strongly Raman active vibron modes in all phases involve in-phase stretches

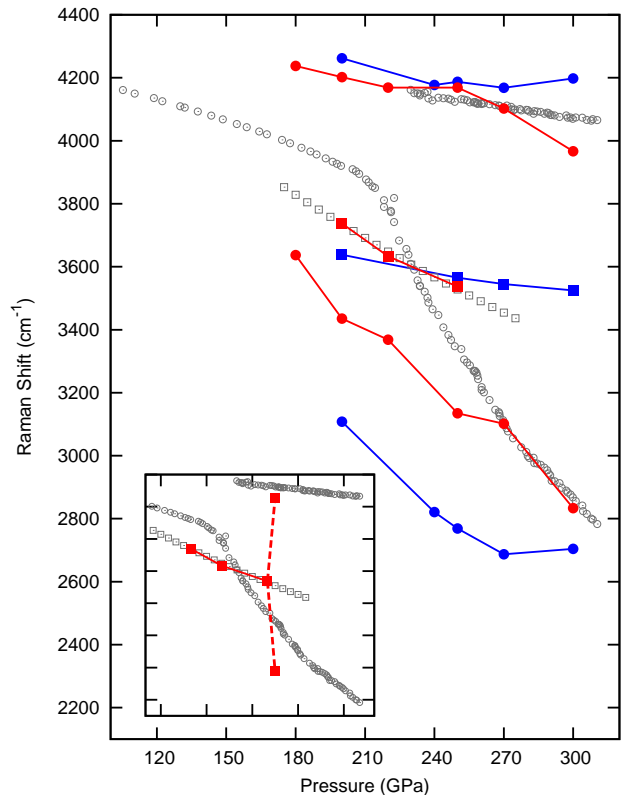


FIG. 3. Pressure dependence of the vibron peaks. (a) experiment: phase IV, 300 K [16] (open grey circles), phase III, 90 K [23] (open grey squares) (b) MD: initialised in *Pc* at 220 K (solid red circles) and in *C2/c* at 220 K (solid red squares) (c) Lattice dynamics: in *Pc* (solid blue circles) and in *C2/c* (solid blue squares). The discontinuity in the *Pc*-MD at 270 GPa corresponds to the IVa-IVb transition. Inset: the bifurcation of the *C2/c*-MD at 250 GPa corresponds to the two Raman peaks which were calculated after *C2/c* was heated to 300 K and it transformed to a distorted structure similar to phase IV.

of the molecules in the *G* and *B* layers. Therefore we make the ansatz that, independent of molecular orientation, the Raman-active vibron modes will involve in-phase stretches. Extracting the Raman signal from the MD is now achieved by identifying molecular bondlengths at each step, which turns out to be always straightforward, and taking the time FT of the average projection of the velocity over the bondlengths [27]. We note that this procedure requires well defined molecules, but does not require us to identify layers [30]. This method produces well-defined peaks, and an example of the fit between simulated and experimental data at 270 GPa is shown in Fig.2.

In Figure 3 we show the pressure dependence of the MD-calculated Raman vibron frequencies compared with the experimental data. In phase III the MD has spectacular agreement with experiment [23]. DFPT gives similar

frequencies, but with a much lower slope (Fig.3). The simulation which started in $C2/c$ at 250 GPa/ 220 K was also driven through the phase transition by heating to 300 K, where it formed a frustrated monoclinic, $GBGB$ -stacked structure [27] leading to the appearance of a second vibron: this structure has mixed-layer character like phase IV, but the frequencies are clearly not in agreement with experiment (Inset to Fig.3).

Figure 3 also shows that the IVb structure with rotating trimers does correctly reproduce the experimental frequencies, while IVa and Pc structures do not. The phase IVb lower peak seems to be comprised of two overlapping peaks (Fig.2 and [27]). We can project the symmetric stretch modes layer by layer: for phase IVb with three different layers, this gives three different frequencies. The near-equal strength of the G' and G'' peaks is due to having one layer of each in the simulation. This ratio is determined by finite size, and in reality the lower peak may be weaker. In fact, this feature is also probably present as a shoulder in the experiment, although its effect could be interpreted as an extended peak width (see Fig. 2). We therefore identify our phase IVb with the experimentally observed phase. IVa occurs in a region of PT space occupied by phase III, so we regard it as metastable.

The analysis of the detailed molecular motions gives a clear, intuitive picture of the high pressure phase behaviour of hydrogen. At low temperature we observe a series of G layers to be the stable structure. Above 60 K molecular motion means that this layer has 3-fold symmetry, but at 0 K a symmetry-breaking distortion freezes in giving the $C2/c$ structure. At a temperature of around 250-300 K (depending on pressure [27]) the transformation to phase IV (our IVb) occurs. The explanation for the entropy-driven transition is evident in the rapid rotational movement of the B layer atoms. The molecules rotate rapidly in the B layer such that their time-averaged positions have hexagonal symmetry. These rotations provide the entropy difference between phases III and IV. At higher temperature, the fast rebonding in the G'' layers enables the rotation of the hexagonal motifs and adds to the entropy, stabilising the IVb structure. Once this rotation begins, the non-rotating G layer adopts hexagonal symmetry. At lower temperatures, no rotation occurs and the hexagonal motifs are distorted and symmetry-broken, as in Pc .

Our 288-atom results are significantly different from previous MD work [31, 32] which has been equivocal about the structure of phase IV, due reorienting of molecules, transformation of one layer type to another, and “mixed” phases of apparently random B and G layer stacking. In our own calculations with 24 or 48 atoms per unit cell we find the same behavior as described in [31, 32].

A simple 1D model [27] of independent layers shows that the continual layer transformation (random layer

stacking) is to be expected from finite size effects, rather than phase stability.

Proton “diffusion” in the G -layers requires two distinct steps:

- Rebonding within the rotating hexagonal motifs, a local process which can contribute to Raman broadening and may be enhanced by tunnelling. This is seen in all simulation sizes at sufficient temperature and illustrated in Figure 1.
- Rearrangement of the motifs themselves, a process which must occur system-wide, and is seen only in 48 atom simulations and smaller.

The rebonding and rotation of these motifs was also described by Liu et al [31], who also showed large diffusion of hydrogen which implies the rearrangement step.

The 48 atom cell has 2×2 trimer hexagons in a G layer, and we also observe correlated changes in the identity of pairs in these motifs, which combined with trimer rotation results in rapid diffusion of hydrogen through the system. This effect is not observed in our 288 atom simulations where the equivalent mechanism would require correlated changes in four trimers: we regard the apparent rapid diffusion in 48-atom simulations phase IV as a finite size effect [33, 34].

Our IVb structure is the best model for the observed phase IV. Our molecule-based technique shows vibron peaks appear which can be associated with each layer type. the B -layer gives the highest frequency, and analysis of the Raman active modes associated with G' and G'' layers in IVb gives two distinct vibrons of slightly different frequency. In the overall pattern, these peaks overlap to give a single peak with a shoulder. The wide variety of environments in which the G -layer molecules find themselves leads to a very broad Raman width. The B layer molecules are well defined and the Raman peak associated with them is sharper. In Pc , IVa and IVb the B -layer vibron has similar frequency, however the G layer modes are quite different.

In sum, we have shown how Raman frequencies can be extracted from molecular dynamics data allowing direct comparison to experiment. We have applied the method to hydrogen at high pressure, showing that the anharmonicity is so extreme as to invalidate use of DFPT normal modes, but that in-phase vibrons are the appropriate coordinates for projection. Our simulations show several different phases, some of which are doubtless metastable, but by comparison to experiment we identify phase III with a structure similar to $C2/c$, and phase IV with a high-entropy hexagonal structure of rotating molecules and trimer motifs. Our simulations give no support to the notions that phase IV exhibits either proton transfer, proton tunneling or mixed molecular and atomic character.

We acknowledge E. Gregoryanz for numerous useful discussions and EPSRC for a studentship (IBM).

-
- [1] F.A. Gorelli, S.F. Elatresh, C.L. Guillaume, M. Marqués, G.J. Ackland, M. Santoro, S.A. Bonev and E. Gregoryanz, *Phys. Rev. Lett.* **108**, 055501 (2013).
- [2] M. Marqués, M. McMahon, E. Gregoryanz, M. Hanfland, C.L. Guillaume, C.J. Pickard, G.J. Ackland and R.J. Nelmes, *Phys. Rev. Lett.* **106**, 095502 (2011).
- [3] D. Porezag and M.R. Pederson, *Phys. Rev. B* **54**, 7830 (1996).
- [4] S. Baroni, S. de Gironcoli, A. Dal Corso and P. Gianozzi, *Rev. Mod. Phys.* **73**, 515 (2001).
- [5] K. Refson, S.J. Clark and P.R. Tulip, *Phys. Rev. B* **73**, 155114 (2006).
- [6] G.J. Ackland, M.C. Warren and S.J. Clark, *J. Phys. CM.* **9**, 7861 (1997).
- [7] C.Z. Wang, C.T. Chan and K.M. Ho, *Phys. Rev. B* **42**, 11276 (1990).
- [8] U. Pinsook and G.J. Ackland, *Phys. Rev. B* **59**, 13642 (1999).
- [9] J. Thomas, J. Turney, R. Iutzi, C. Amon, A. McGaughey, *Phys. Rev. B* **81**, 081411(R) (2010).
- [10] T. Lan, X. Tang, and B. Fultz, *Phys. Rev. B* **85**, 094305 (2012).
- [11] P. Souvatzis, S. Arapan, O. Eriksson, M. Katsnelson, *Europhysics letters* **96**, 66006 (2011).
- [12] S. Scandalo, *Proc. Natl. Acad. Sci. U.S.A.* **100**, 3051 (2003).
- [13] J.Kohanoff, S. Scandalo, G.L. Chiarotti and E. Tosatti, *Phys. Rev. Lett.* **78**, 2783 (1997).
- [14] J.Kohanoff, S. Scandalo, S. de Gironcoli and E. Tosatti, *Phys. Rev. Lett.* **83**, 4097 (1999).
- [15] H.K. Mao and R.J. Hemley, *Rev. Mod. Phys.* **66**, 671 (1994).
- [16] R.T. Howie, C.L. Guillaume, T. Scheler, A. F. Goncharov, and E. Gregoryanz, *Phys. Rev. Lett.* **108**, 125501 (2012).
- [17] C.J. Pickard, M. Martinez-Canales and R.J. Needs, *Phys.Rev.B* **85**, 214114 (2012), erratum: *Phys.Rev. B* **86**, 059902(E).
- [18] C.J. Pickard and R.J. Needs, *Phys. Rev. Lett.* **97**, 045504 (2006).
- [19] C.J. Pickard and R.J. Needs, *Nature Phys.* **3**, 473 (2007).
- [20] R.T. Howie, T. Scheler, C.L. Guillaume and E. Gregoryanz, *Phys. Rev. B* **86**, 214104 (2012).
- [21] X.-Z. Li, B. Walker, M.I.J. Probert, C.J. Pickard, R.J. Needs and A. Michaelides, *J. Phys. CM.* **25**, 085402 (2013).
- [22] M. Morales, J. McMahon, C. Pierleoni and D. Ceperley, *Phys. Rev. Lett.* **110**, 065702 (2013).
- [23] Y. Akahama, H. Kawamura, N. Hirao, Y. Ohishi and K. Takemura, *J. Phys.: Conf. Ser.* **215** 012056 (2010).
- [24] Y. Akahama, M. Nishimura, H. Kawamura, N. Hirao, Y. Ohishi and K. Takemura, *Phys. Rev. B* **82**, 060101(R) (2010).
- [25] P. Loubeyre, F. Occelli and R. Letoullec, *Nature* **416**, 613 (2002).
- [26] C.-S. Zha, Z. Liu, and R.J. Hemley, *Phys. Rev. Lett.* **108**, 146402 (2012).
- [27] Check Supplementary Materials for further details.
- [28] M.D. Segall, P.J.D. Lindan, M.J. Probert, C.J. Pickard, P.J. Hasnip, S.J. Clark and M.C. Payne, *J. Phys. CM.* **14**, 2717 (2002).
- [29] We note that convergence of the Raman signal requires a much higher k -point sampling than either structure or phonon calculations.
- [30] It is possible to identify the layers, and to project only onto molecules in one layer. Each different layer produces a single peak: the higher frequency peak is associated with the B layers. However, there is interference between similar layers, so the sum of the layer projections does not give the correct Raman signal.
- [31] H.Liu and Y.Ma, *Phys.Rev.Lett.* **110**, 025903 (2013); H. Liu, L. Zhu, W. Cui and Y. Ma, *J. Chem. Phys.* **137**, 074501 (2012).
- [32] A.F. Goncharov, J.S. Tse, H. Wang, J. Yang, V.V. Struzhkin, R.T. Howie and E. Gregoryanz, *Phys. Rev. B* **87**, 024101 (2013).
- [33] M.A. Morales, C. Pierleoni, E. Schwegler and D.M. Ceperley, *Proc. Natl. Acad. Sci. U.S.A.* **107**, 12 799 (2010).
- [34] W. Lorenzen, B. Holst and R. Redmer, *Phys. Rev. B* **82**, 195107 (2010).
- [S1] J.P. Perdew, K. Burke, and M. Ernzerhof, *Phys. Rev. Lett.* **77**, 3865 (1996).
- [S2] Using the input string: “H 0—0.7—2—6—8—10L(qc=10)” in the CASTEP parameter file.

SUPPLEMENTARY MATERIALS

Finite Temperature Phonons by projection onto normal modes

In order to study a particular vibrational mode in a crystal, we first define the calculation supercell, and relax the structure at 0 K. The atoms are now located at positions given by $3N$ cartesian coordinates X_j . We regard the supercell as a non-primitive unit cell, in which case X_j are the basis positions.

We now do a lattice dynamics calculation at 0 K using either finite displacements (Ref. [6] from the paper) or DFPT (Ref. [5] from the paper). This gives us a set of normal mode coordinates e_i . With each of these normal modes we can calculate harmonic phonon frequency (ω_i), Raman activity and oscillator strength (R_i), IR activity and oscillator strength. i runs from 1 to $3N$, the number of normal modes. all of this is already standard in CASTEP.

From an MD simulation with T timesteps we generate trajectories of the atoms, $x_i(t)$, at finite temperature. We can expand each cartesian component of the trajectory in terms of the normal modes (ignoring translations).

$$x_j(t) = X_j + \sum_{i=4}^{3N} \alpha_i(t) e_{ij}$$

So far all this is exact, we just made a linear transformation of the coordinate system. $\alpha_i(t)$ is fully determined by the MD. Similarly for velocities:

$$\dot{x}_j(t) = \sum_{i=4}^{3N} \dot{\alpha}_i(t) e_{ij}$$

Now we assume that we are in the harmonic regime.

$$\alpha_i(t) = Re \left[a_i \exp^{i(\omega_i t + \phi_i)} \right] \quad (1)$$

$$\dot{\alpha}_i(t) = Im \left[a_i \omega_i \exp^{i(\omega_i t + \phi_i)} \right] \quad (2)$$

This assumption means that a_i , ω_i and ϕ_i are independent of time.

It is now straightforward to use the MD data to obtain ω_i , from the FT. The FT of α , is problematic since at high temperature $\langle \alpha \rangle \neq 0$, but the same information is present in $\dot{\alpha}$ which is more convenient since $\langle \dot{\alpha} \rangle = 0$. In the harmonic limit $FT[\dot{\alpha}_i(t)]$ is simply a delta function at $\omega = \omega_i$.

Note we have NOT used the frequencies from the lattice dynamics, we have calculated them from the MD. In the harmonic approximation, the same modes will be Raman/IR Active in the MD as in the lattice dynamics. As usual, we can calculate the occupied phonon density of states from the velocity autocorrelation function:

$$FT \left[\sum_j \dot{x}_j(t) \dot{x}_j(0) \right] = FT \left[\sum_i \sum_j \dot{\alpha}_i(t) \dot{\alpha}_i(0) e_{ij}^2 \right]$$

By analogy, the total Raman signal becomes:

$$FT \left[\sum_{ij} R_i \dot{\alpha}_i(t) \dot{\alpha}_i(0) e_{ij} \right]$$

and we can obtain the mode frequency for each mode i from the peak in: $FT[\dot{\alpha}_i(t) \dot{\alpha}_i(0)]$.

In the harmonic limit, the Raman signal is simply the sum of individual modes.

All of this has been applied in classical MD by numerous authors, e.g. Ref. [8] from the paper. We now, consider applying exactly the same process to an anharmonic MD. Modes with strong Raman/IR signals will still have strong Raman signals, since the polarisability ultimately depends on the motion of the atoms.

There are some issues about the magnitude of the oscillations. In the harmonic case it will never equilibrate. To get close to equilibrium it seems sensible to set initial displacements and velocities based on temperature from the normal modes (with random phase ϕ).

$$\alpha_i(t=0) = \sqrt{kT/m\omega_i^2} \sin(\phi)$$

$$\dot{\alpha}_i(t=0) = \sqrt{kT/m} \cos(\phi)$$

This is done, e.g. in SCAILD (Ref. [11] from the paper), but not automatically in CASTEP. This could be important in evaluating Raman intensities and line widths, since the anharmonic effects will depend on the phonon amplitude. However, for high pressure studies the experimental Raman intensities depend strongly on the apparatus and are not used quantitatively.

For H_2 vibrons the Raman activity comes from the symmetric molecular stretch. It is therefore necessary to associate α not with fixed normal modes, but with the molecule stretches:

$$\alpha(t) = \sum_j \mathbf{r}_j(\mathbf{t}) - \mathbf{r}_{j_m}(\mathbf{t})$$

where $\mathbf{r}_{j_m}(t)$ is the vector position of the molecular partner atom to j , at time t .

This requires us to identify molecules at each time step t (i.e. molecule labelling might change during the simulation, which could cause discontinuities in the velocity functions). Since the stretching modes can change at each time step, $\dot{\alpha}(t)$ is not the simple time derivative of $\alpha(t)$, but can be calculated by projecting the velocity $v_j(t)$ of each atom onto the stretching mode. Finally, the spectrum for the vibron modes is:

$$FT \left[\sum_j \mathbf{v}_j(\mathbf{t}) \cdot [\mathbf{r}_j(\mathbf{t}) - \mathbf{r}_{j_m}(\mathbf{t})] \right]$$

Here we investigate vibrons, but the method is completely general provided that the Raman-active molecular mode can be identified. To validate our code, we performed an MD simulation at 60 K starting in the Pc structure. Figure 5 shows very good agreement in this simple regime where only harmonic effects are present. The MD projection onto normal modes or symmetric stretches give indistinguishable results.

Finite size effects and a simplified layer model for dense H_2

We have seen that the primary feature of the structural hierarchy is the layer, the secondary feature is the interaction between layers, and that interactions beyond this are weak. From the MD we note that adjacent B layers are not observed, presumably high in energy, while numerous relative translations of the G layers are observed, depending on kinetics: this implies little energy preference.

It is possible to understand the transition using a simple 1D model. We assign differences in energies ($U_{GB} = U_G - U_B < 0$ and entropies $S_{GB} = S_G - S_B < 0$) to each layer, and a layer interaction J_{ij} where i and j represent G or B layers. In this model the free energies of various N atom supercells with L layers are given in table I.

Phase	Stacking	Free energy
III	all-G	$N(U_G - TS_G + J_{GG})$
I	all-B	$N(U_B - TS_B + J_{BB})$
IV	GBGB	$N(U_B - TS_B + U_G - TS_G + J_{GB})/2$
	random	$N(2U_B - 2TS_B + 2U_G - 2TS_G + J_{BB} + J_{GG} + 2J_{GB})/4 - LT \ln 2$

TABLE I. Energies of four possible “phases” which could be realised in an L=4 layer supercell, where in the general case L is the number of layers.

Assuming $J_{GG} < J_{GB} < J_{BB}$ this model gives a phase diagram as shown in figure 4, including a III-IV transition and a phase of all freely rotating molecules (rather similar to phase I). As discussed above in the context of 48 atom simulations, random stacking is favoured by the $LT \ln 2$ term, which is significant only for small system sizes where the number of layers is comparable to the number of atoms.

Each layer contains only 12 atoms. For a free energy difference of F_{BG} per atom between the distinct layer types, Boltzmann statistics shows that the probability of finding the B layer is $1/(1 + \exp(-12F_{BG}/KT))$. Static calculation implies a $F_{BG} \approx 2\text{meV/atom}$, so at 300 K the unfavoured layer is present 28% of the time.

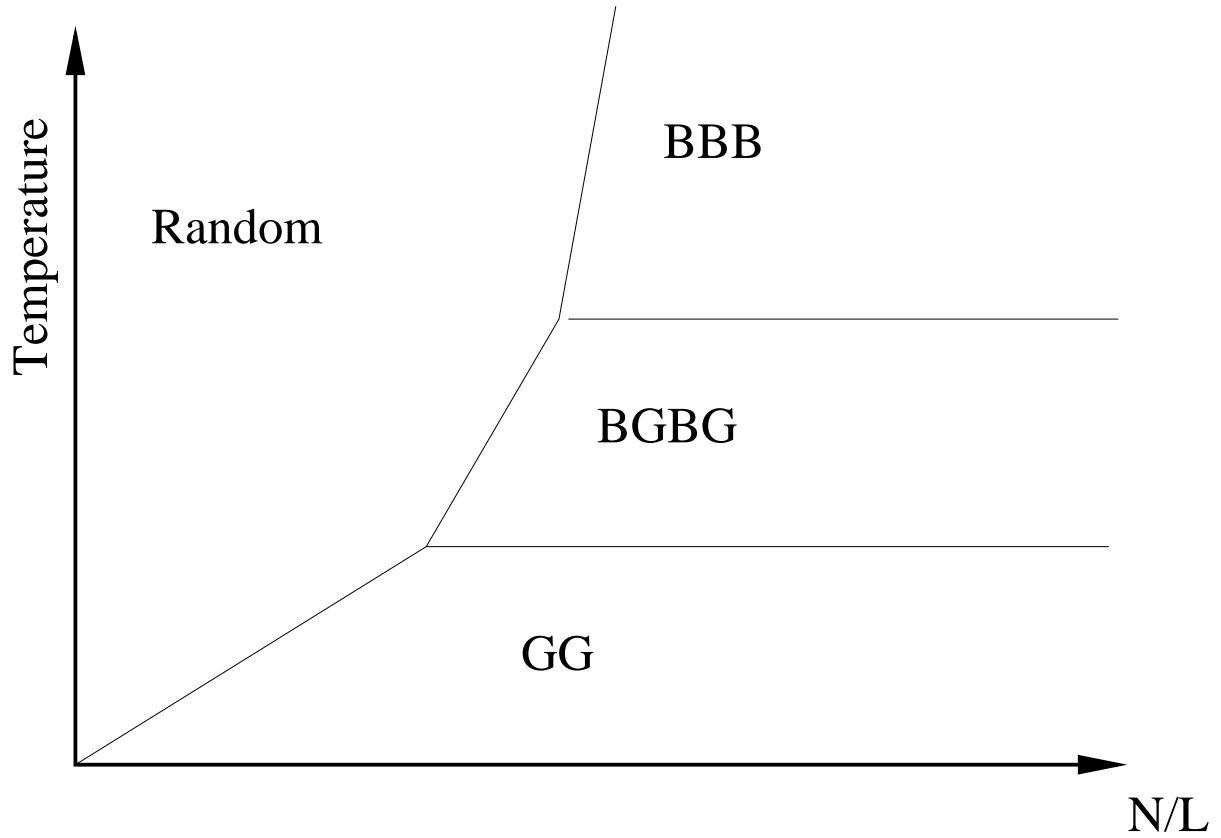


FIG. 4. Schematic drawing of the effect of finite size and temperature for the simple layer model. *Random* represents the phase observed in simulations with 24 or 48 atoms, *BB*, *BGBG*, and *GGG* are similar to phases III, IV and I respectively. For small enough systems (low N/L) randomly oriented layers will always be stable, however in the thermodynamic limit $N/L \rightarrow \infty$ the phase sequence increasingly favours free-rotor *B*-layers, the mixed layer appearing whenever *BB* interactions are strongly disfavoured. The actual values of T and N/L at the phase boundary depend on the parameters, which in turn depend on pressure and temperature.

Calculation details

Data was collected from DFT calculations using the CASTEP package. The MD calculations involved 288 atoms initiated in prerelaxed monoclinic supercells of either Pc ($\beta \approx 91^\circ$) or $C2/c$ ($\beta \approx 144^\circ$) structures, and used a constant-stress Parrinello-Rahman barostat. Observed phase transitions involved small changes of cell shape, but nothing close to the 53° change required to go from Pc to $C2/c$.

We used the PBE exchange correlation functional which has become the standard for work in hydrogen [S1]. Two different pseudopotentials were developed, an ultrasoft (300eV cut off) generated “on the fly” [S2] for the molecular dynamics and a harder norm-conserving pseudopotential (1200eV cut off) for which Raman calculations are more easily carried out. The structural results obtained were similar for the two methods. For the DFPT lattice dynamics a single unit cell k-point set of $9 \times 5 \times 5$ was used, giving 69 independent k-points.

Norm conserving Pc	a	b	c	vibrons	
P					
200	2.986	5.207	5.324	3108	4262
220	2.949	5.129	5.259	2929	4208
240	2.915	5.071	5.202	2821	4177
250	2.896	5.054	5.163	2845	4187
270	2.868	4.989	5.121	2684	4168
300	2.826	4.917	5.048	2597	4157
350	2.767	4.815	4.940	2549	4136
USP Pc	a	b	c		
P					
180	3.031	5.272	5.405		
200	2.986	5.194	5.329		
250	2.894	5.051	5.165		
300	2.823	4.929	5.033		
C2c	a	b	c	β	vibron
P					
200	5.221663	2.976715	4.379227	142.433942	3638.156521
230	5.126252	2.920341	4.297475	142.467436	3589.690041
250	5.069649	2.887193	4.249310	142.485532	3564.867343
270	5.017617	2.856906	4.205190	142.501804	3545.228906
300	4.9468405	2.8159880	4.145307	142.524403	3524.644474

TABLE II. Structural details from static relaxations of Pc and $C2/c$ structures. These structures were used for DFPT-LD calculation, and to initialise the MD calculations

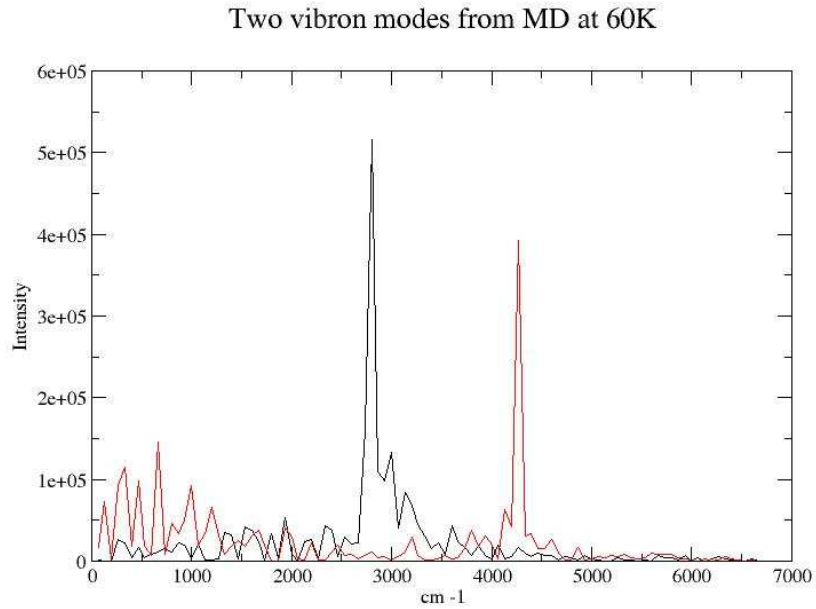


FIG. 5. Fourier transform of projected velocity autocorrelation function of Raman active normal mode. The two Raman-active vibron modes were chosen, and can be seen to be in excellent agreement with lattice dynamics values 2845 cm^{-1} and 4187 cm^{-1} . From MD calculation on Pc at 250 GPa, 60 K. Data in Fig.2 were obtained from peaks in graphs such as this.

No.	Initial Structure	Atoms	Ensemble	Number of Iterations	Time Step	Pressure	Temperature
1	Pc	48	NVE	9000	0.5 fs	250 GPa	60 K
2	Pc	48	NVE	6000	0.5 fs	250 GPa	145 K
3	Pc	48	NVE	6000	0.5 fs	250 GPa	215 K
4	Pc	48	NVE	6000	0.5 fs	250 GPa	285 K
5	Pc	48	NVE	6000	0.5 fs	250 GPa	360 K
6	Pc	48	NVE	6000	0.5 fs	250 GPa	430 K
7	Pc	48	NVE	6000	0.5 fs	250 GPa	500 K
8	Pc	288	NVE	3000	0.5 fs	250 GPa	145 K
9	Pc	288	NVE	3000	0.5 fs	250 GPa	215 K
10	Pc	288	NVE	3000	0.5 fs	250 GPa	285 K
11	Pc	288	NVE	3000	0.5 fs	250 GPa	360 K
12	Pc	288	NVE	3000	0.5 fs	250 GPa	430 K
13	Pc	288	NVE	3000	0.5 fs	250 GPa	500 K
14	Pc	288	NPT + NVE	500 + 1500	0.5 fs	180 GPa	220 K
15	Pc	288	NPT + NVE	500 + 1500	0.5 fs	200 GPa	220 K
16	Pc	288	NPT + NVE	500 + 1500	0.5 fs	220 GPa	220 K
17	Pc	288	NPT + NVE	500 + 1500	0.5 fs	250 GPa	220 K
18	Pc	288	NPT + NVE	500 + 1500	0.5 fs	270 GPa	220 K
19	Pc	288	NPT + NVE	500 + 1500	0.5 fs	300 GPa	220 K
20	C2/c	288	NPT + NVE	500 + 1500	0.5 fs	200 GPa	220 K
21	C2/c	288	NPT + NVE	500 + 1500	0.5 fs	220 GPa	220 K
22	C2/c	288	NPT + NVE	500 + 1500	0.5 fs	250 GPa	220 K
23	GGGG stacking	288	NPT	7 x 200 + 6 x 200	0.5 fs	250 GPa	100 K \rightarrow 400 K (+50 K) 350 K \rightarrow 100 K (-50 K)
24	C2/c	288	NPT	400 + 600 + 200	0.5 fs	250 GPa	200 K \rightarrow 300 K \rightarrow 400 K
25	C2/c	288	NPT + NVE	800 + 2000	0.5 fs	250 GPa	300 K

TABLE III. Summary of MD calculations.

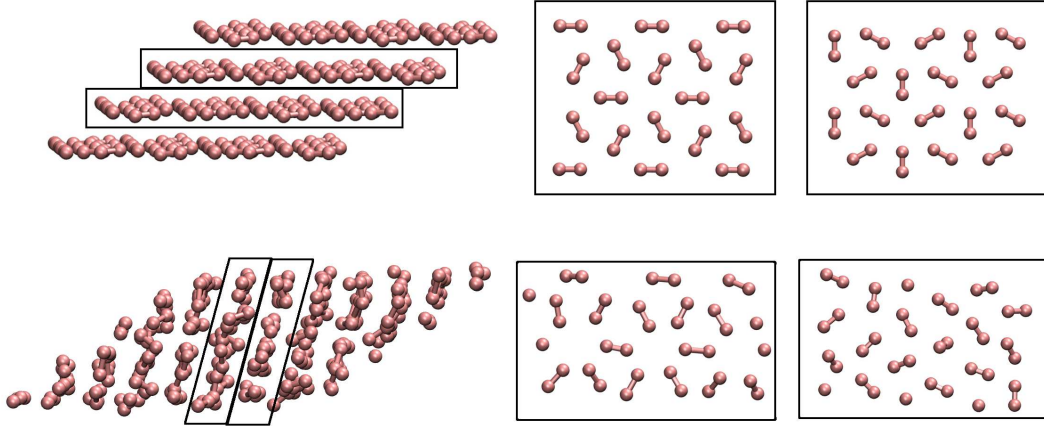


FIG. 6. Phase III transformation observed in NPT MD initialized in $C2/c$ structure and heated at 250 GPa (see simulation 24 from Table III and Fig. 11). Left side shows MD supercell, while right side shows the corresponding layers. Top structure is Pickard's $C2/c$ (Ref. [19] from the paper) relaxed at 250 GPa, while bottom structure is a snapshot from MD, after the transformation has occurred: the G -layer stacking of the $C2/c$ at the top is clear. The alternating $BGBG$ stacking in the high temperature phase (lower) is similar to phase IV, but there is some frustration, which leads to a lower Raman-mode frequency (around 2980 cm^{-1}). The frustration illustrates the hierarchical nature of the bonding: a primary tendency to form layers, secondary to order as B or G within the layers, and a tertiary effect of interlayer interactions.

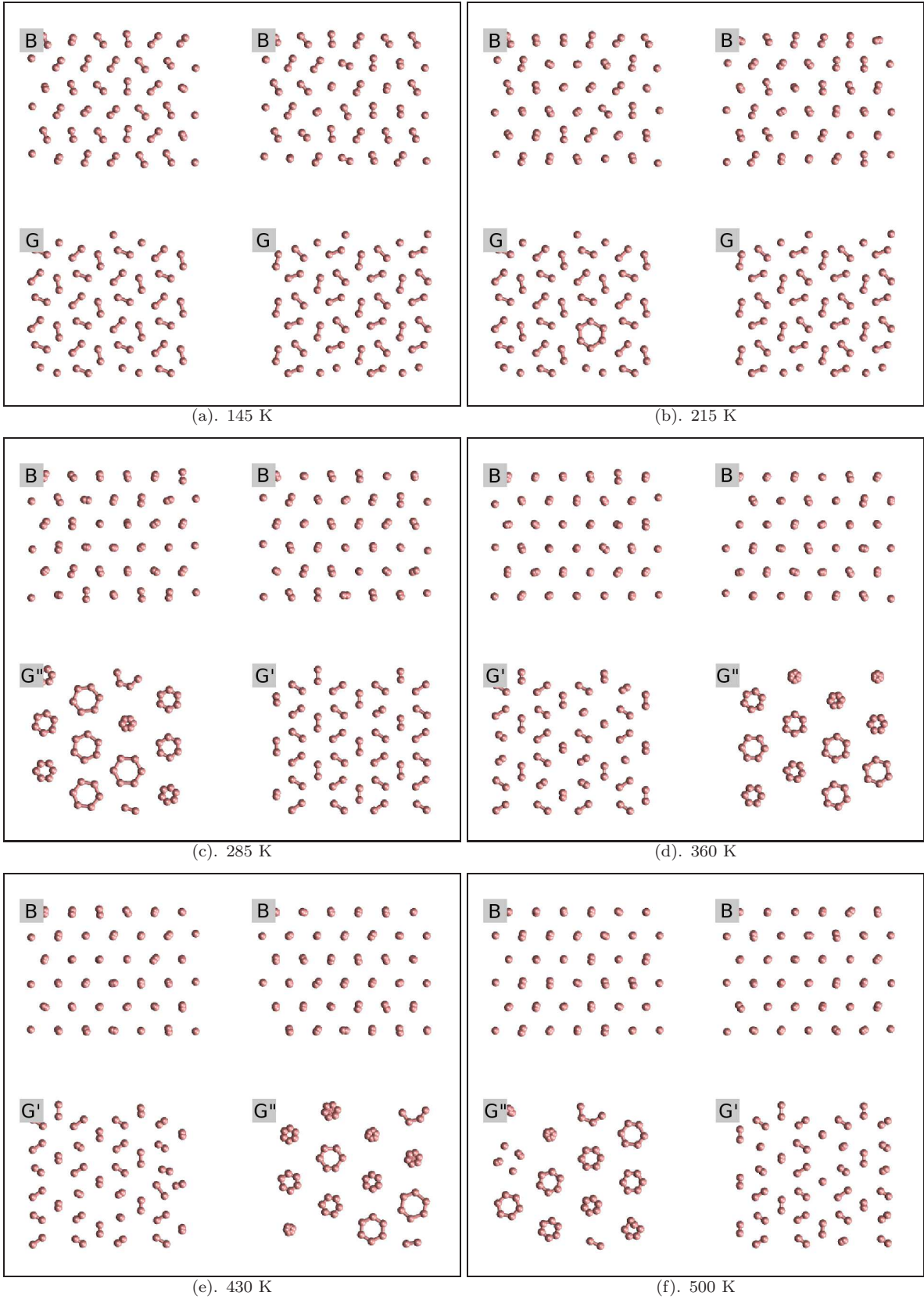


FIG. 7. As per figure 1 in the main paper, average positions of atoms over 1.5ps at 250 GPa and temperatures (from top left) 145 K, 215 K, 285 K, 360 K, 430 K, 500 K. Stacking is $BGBG$ and $BG'BG''$, respectively.

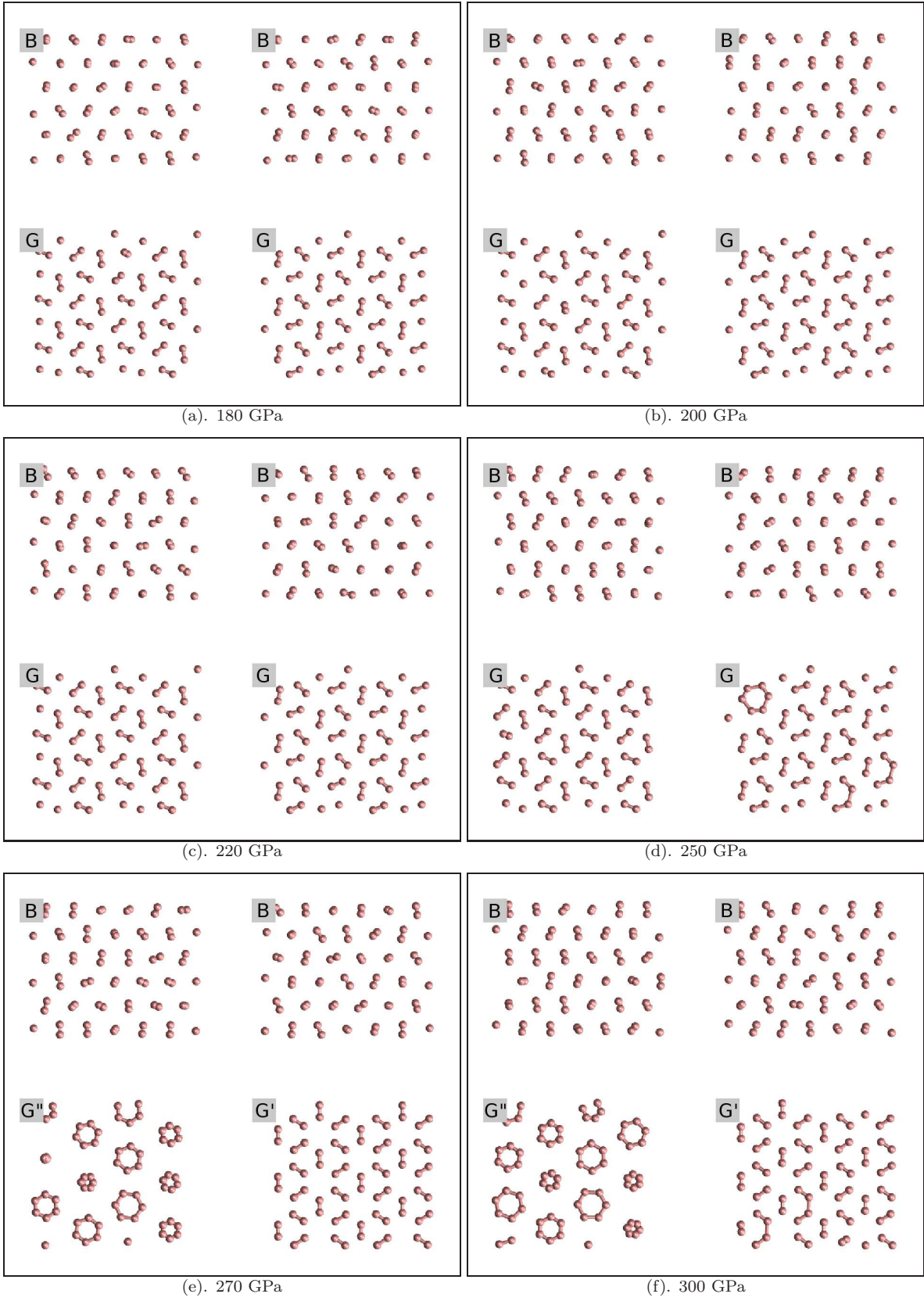


FIG. 8. As per figure 1 in the main paper, average positions of atoms over 1ps at 220 K and pressures (from top left) 180 GPa, 200 GPa, 220 GPa, 250 GPa, 270 GPa, 300 GPa. Stacking is $BGBG$ and $BG'BG''$, respectively.

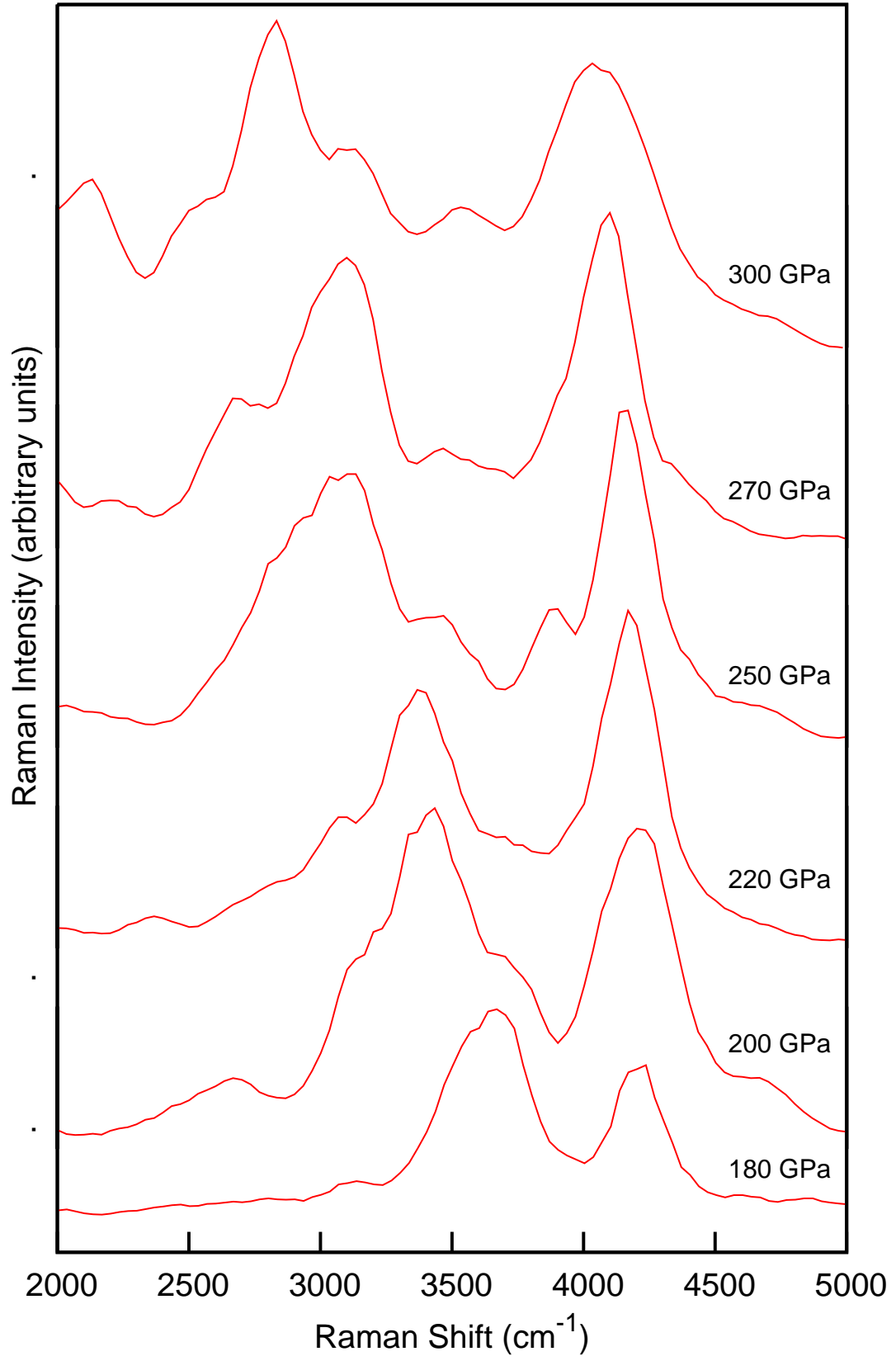


FIG. 9. Calculated Raman peaks from MD at 220 K for a range of pressures traversing the VIa-VIb transition between 250 GPa and 270 GPa.

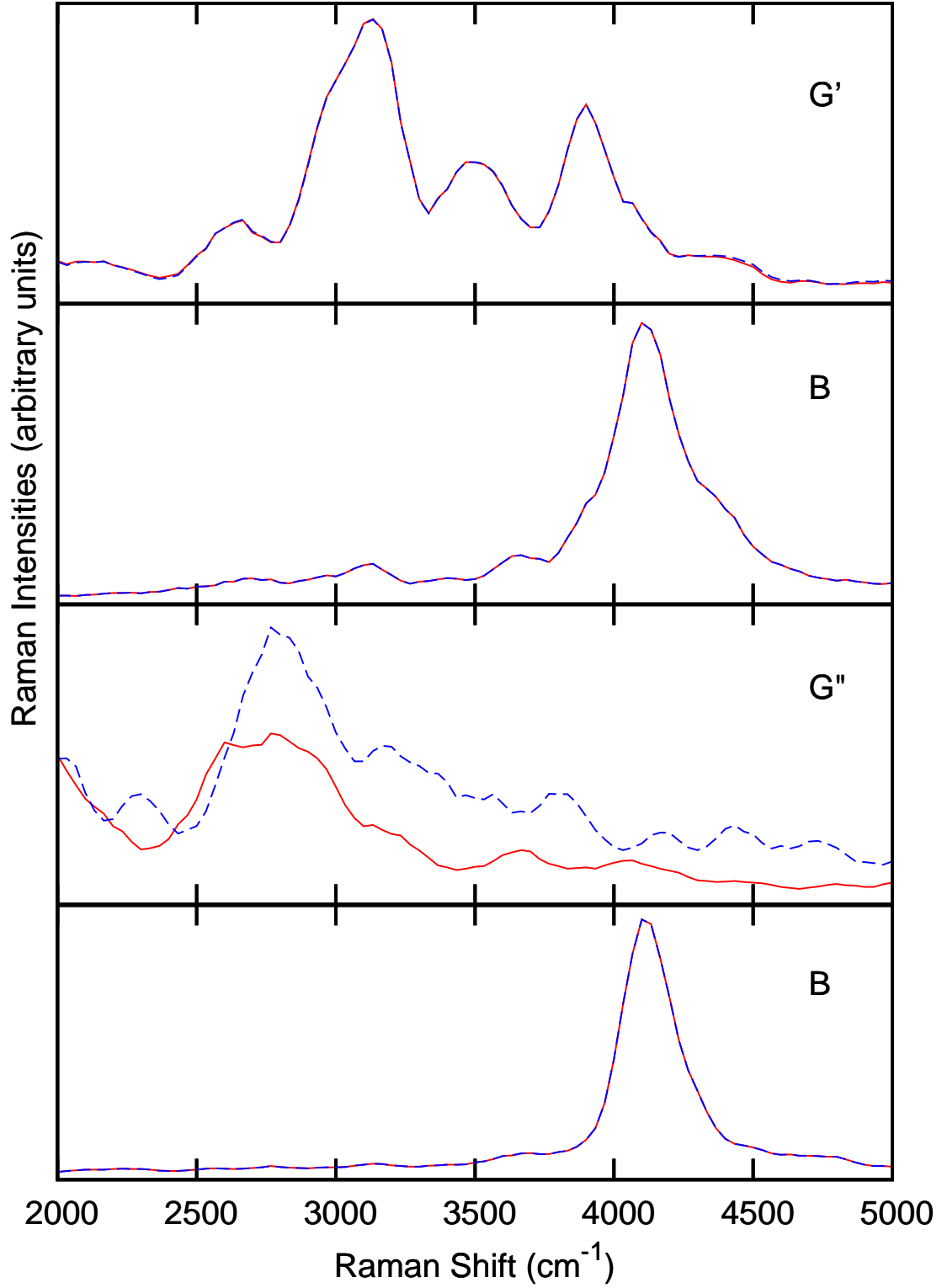


FIG. 10. Calculated Raman peaks from MD started in Pc at 220 K, 270 GPa, individually for each layer with two different methods: identifying molecules at $t = 0$ and keeping the same labels throughout the simulation (red), identifying molecules at each time step (blue). For B and G' layers the same results are found, while G'' gives very different results depending on the method, suggesting continuous rebonding. Note that the sum of the four spectra will be slightly different from the spectrum of the whole structure, for which the complex FT phases have to be taken into account.

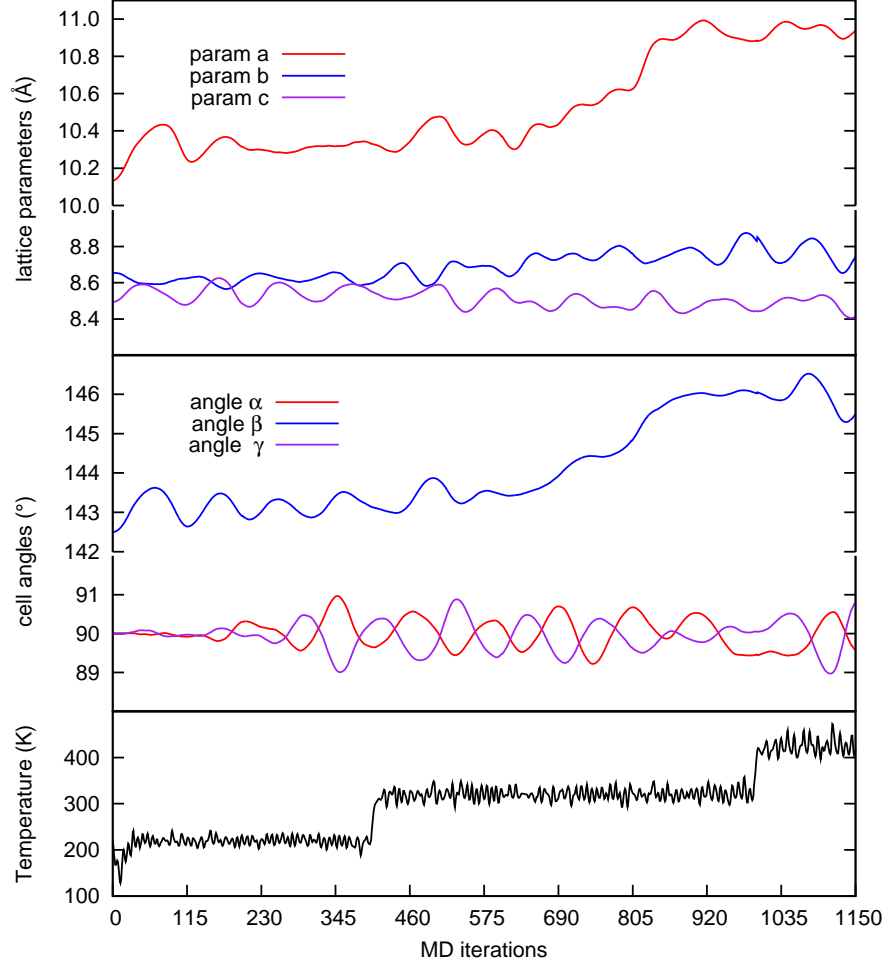


FIG. 11. Figure showing lattice parameters and angles for a long MD run with a ramped temperature rise, started in the $C2/c$ structure (see simulation 24 from Table III and Fig. 6). The phase transition from III-IV appears evident, however close comparison of Raman data with experiment reveals that the high-T phase is not consistent with experiment. Parrinello-Rahman dynamics is not able to achieve the massive cell-shape change required to reach phase IVb.

Phase	symmetry	conditions	description
gas		ambient	molecular H_2
I	hcp	low-T + pressure	quantum rotation of H_2 molecules.
II	distorted hcp	Low temperature, <150 GPa	symmetry-breaking distortion of I
III	$C2/c$	150+ GPa 300- K	layer molecules arranged in hexagonal trimers.
IV		200+ GPa, ambient temperature	hexagonal and free-rotating molecular layers

TABLE IV. Summary of known properties of phases on hydrogen; phase boundaries in hydrogen are not yet definitively established.